
Deep Partial Updating

Zhongnan Qu
ETH Zurich
quz@ethz.ch

Cong Liu*
UT Dallas
cong@utdallas.edu

Junfeng Guo
UT Dallas
gjf199509236817@gmail.com

Lothar Thiele
ETH Zurich
thiele@ethz.ch

Abstract

Emerging edge intelligence applications require the server to continuously retrain and update deep neural networks deployed on remote edge nodes in order to leverage newly collected data samples. Unfortunately, it may be impossible in practice to continuously send fully updated weights to these edge nodes due to the highly constrained communication resource. In this paper, we propose the weight-wise deep partial updating paradigm, which smartly selects only a subset of weights to update at each server-to-edge communication round, while achieving a similar performance compared to full updating. Our method is established through analytically upper-bounding the loss difference between partial updating and full updating, and only updates the weights which make the largest contributions to the upper bound. Extensive experimental results demonstrate the efficacy of our partial updating methodology which achieves a high inference accuracy while updating a rather small number of weights.

1 Introduction

To deploy deep neural networks (DNNs) on resource-constrained edge devices, extensive research has been done to compress a well-trained model via pruning [7, 21] and quantization [6, 20]. During on-device inference, compressed networks may achieve a good balance between model performance (*e.g.*, prediction accuracy) and resource demand (*e.g.*, memory, computation, energy). However, due to the lack of relevant training data or an unknown sensing environment, pre-trained DNN models may not yield satisfactory performance. Retraining the model leveraging newly collected data (from edge devices or from other sources) is needed for desirable performance. Example application scenarios of relevance include vision robotic sensing in an unknown environment (*e.g.*, Mars) [15], local translators on mobile phones [2], and acoustic sensor networks deployed in Alpine environments [16].

It is mostly impossible to perform on-device retraining on edge devices due to their resource-constrained nature. Instead, feasible retraining in practice often occurs on a remote server with sufficient resource. One possible strategy to achieve retraining in this case is a two-stage iterative process: (i) at each round, edge devices collect new data samples and send them to the server, and (ii) the server retrains the network using all collected data, and then sends the updates to each edge device [3]. An essential challenge herein is that the transmissions in the second stage are highly constrained by the limited communication resource (*e.g.*, bandwidth, energy) in comparison to the first stage. State-of-the-art DNN models always require tens or even hundreds of mega-Bytes (MB) to store parameters, whereas a single batch of data samples (a number of samples that can lead to reasonable updates in batch training) needs a relatively smaller amount of data. For example, for

*Corresponding Author: Cong Liu.

CIFAR10 dataset [12], the weights of a popular VGGNet require 56.09MB storage, while one batch of 128 samples only uses around 0.40MB [24, 6, 20].

Besides, edge devices could decide on and send only critical samples with active learning schemes [25, 1]. The server may also receive training data from other sources, *e.g.*, through data augmentation or new data collection campaigns. These considerations indicate that the updated weights which are sent to edge devices by the server at the second stage become a major bottleneck.

To resolve the above challenges pertaining to updating the network, we propose to partially update the network through changing only a small subset of the weights at each round. Doing so can significantly reduce the server-to-device communication overhead. Furthermore, fewer parameter updates also lead to less memory access on edge devices, which in turn results in a smaller energy consumption [10]. Our goal of performing partial updating is to determine which subset of weights shall be updated at each round, such that similar accuracy can be achieved compared to fully updating all weights.

Our key concept for partial updating is based on the hypothesis, that *a weight shall be updated only if it has a large contribution to the loss reduction* given the newly collected data samples. Specially, we define a binary mask \mathbf{m} to describe which weights are subject to update, *i.e.*, $m_i = 1$ implies updating this weight and $m_i = 0$ implies fixing the weight to its initial value. For any \mathbf{m} , we establish an analytical upper bound on the difference between the loss value under partial updating and that under full updating. We determine an optimized mask \mathbf{m} by combining two different view points: (i) measuring the “global contribution” of each weight to the upper bound through computing the Euclidean distance, and (ii) measuring each weight’s “local contribution” within each optimization step using gradient-related information. The weights to be updated according to \mathbf{m} will be further sparsely fine-tuned while the remaining weights are rewound to their initial values.

Related Work. Although partial updating has been adopted in some prior works, it is conducted in a fairly coarse-grained manner, *e.g.*, layer-wise or neuron-wise, and targets at completely different objectives. Specially, under continual learning settings, [26, 11] propose to freeze all weights related to the neurons which are more critical in performing prior tasks than new ones, to preserve existing knowledge. Under adversarial attack settings, [23] updates the weights in the first several layers only, which yield dominating impact on the extracted features, for better attack efficacy. Under architecture generalization settings, [4] studies the generalization performance through the resulting loss degradation when rewinding the weights of each individual layer to their initial values. Unfortunately, such techniques cannot be applied in our problem setting which seeks to perform fine-grained, *i.e.*, weight-wise, partial updating given newly collected training samples.

Contributions. Our contributions can be summarized as follows.

- We formalize the deep partial updating paradigm, *i.e.*, how to perform weight-wise partial updating of deep neural networks w.r.t. the loss given newly collected training data samples.
- We propose a new approach which determines the optimized subset of weights that shall be selected for partial updating, through measuring each weight’s contribution to the analytical upper bound on the loss reduction.
- Experimental results on three popular vision datasets demonstrate the efficacy of our approach. Particularly comparing to full updating, our approach can achieve a similar accuracy while reducing the size of the transmitted data by 90.4% on average (up to 99.6%).

2 Notation and Setting

In this section, we define the notation used throughout this paper, and provide a formalized problem setting, *i.e.*, deep partial updating. We consider a set of remote edge devices that implement on-device inference. They are connected to a host server that is able to perform network training and retraining. We consider the necessary amount of information that needs to be communicated to each edge device to update its inference network.

Assume there are in total R rounds of network updates. The network deployed in the r^{th} round is represented with its weight vector \mathbf{w}^r . The training data used to update the network for the r^{th} round is represented as $\mathcal{D}^r = \delta\mathcal{D}^r \cup \mathcal{D}^{r-1}$. In other words, newly collected data samples $\delta\mathcal{D}^r$ are made available to the server in round $r - 1$.

In order to reduce the amount of information that needs to be sent to edge devices, only partial weights of \mathbf{w}^{r-1} shall be updated when determining \mathbf{w}^r . The overall optimization problem for weight-wise partial updating in round $r - 1$ can thus be formulated as

$$\min_{\delta \mathbf{w}^r} \quad \ell(\mathbf{w}^{r-1} + \delta \mathbf{w}^r; \mathcal{D}^r) \quad (1)$$

$$\text{s.t.} \quad \|\delta \mathbf{w}^r\|_0 \leq k \cdot I \quad (2)$$

where ℓ denotes the loss function, $\|\cdot\|_0$ denotes the L0-norm, k denotes the defined updating ratio, and $\delta \mathbf{w}^r$ denotes the increment of \mathbf{w}^{r-1} . Note that both \mathbf{w}^{r-1} and $\delta \mathbf{w}^r$ are drawn from \mathbb{R}^I , where I denotes the total number of weights.

In this case, only a fraction of kI weights and the corresponding index information need to be communicated to each edge device for updating the network in round r , namely the partial updates $\delta \mathbf{w}^r$. It is worth noting that the index information is relatively small in size compared to the partially updated weights (see Sec. 4). On each edge device, the weight vector is updated as

$$\mathbf{w}^r = \mathbf{w}^{r-1} + \delta \mathbf{w}^r \quad (3)$$

In order to simplify the notation, we will only consider a single update, *i.e.*, from weight vector \mathbf{w} (corresponding to \mathbf{w}^{r-1}) to weight vector $\tilde{\mathbf{w}}$ (corresponding to \mathbf{w}^r) with

$$\tilde{\mathbf{w}} = \mathbf{w} + \delta \tilde{\mathbf{w}}$$

3 Partial Updating

We develop a two-step approach for resolving the partial updating optimization problem in Eq.(1)-Eq.(2). The final implementation used for the experimental results, see Sec. 4, contains some minor adaptations that do not change the main principles as explained next. In the first step, we compute a subset of all weights with only kI weights. These weights will be allowed to change their values. In the second step, we optimize the weights in the chosen subset in order to minimize the loss function in Eq.(1). The overall approach is depicted in Fig. 1.

The approach for the first step not only determines the subset of weights but also computes the initial values for the second optimization step. In particular, we first optimize the loss function Eq.(1) from initial weights \mathbf{w} with a standard optimizer, *e.g.*, SGD or its variants. As a result, we obtain the minimized loss $\ell(\mathbf{w}^f)$ with $\mathbf{w}^f = \mathbf{w} + \delta \mathbf{w}^f$, where the superscript *f* denotes “full updating”. Of course, the constraint Eq.(2) is not taken into account yet. But the information gathered during this optimization is used to determine the subset of weights that will be changed and therefore, that need to be communicated to the edge devices.

In the explanation of the method in Sec. 3.1, we use the mask \mathbf{m} with $\mathbf{m} \in \{0, 1\}^I$ to describe which weights are subject to change and which ones are not. The weights with $m_i = 1$ are trainable, whereas the weights with $m_i = 0$ will be rewound from the values in \mathbf{w}^f to their initial values in \mathbf{w} , *i.e.*, unchanged. Obviously, we find $\sum_i m_i = k \cdot I$. In summary, the purpose of this first step is to determine an optimized mask \mathbf{m} .

In the second step we start a weight optimization from a network with kI weights from the optimized network \mathbf{w}^f and $(1 - k)I$ weights from the previous, still deployed network \mathbf{w} . In other words, the initial weights for this optimization are $\mathbf{w} + \delta \mathbf{w}^f \odot \mathbf{m}$, where \odot denotes an element-wise multiplication. We still use a standard optimizer. In order to determine the final solution $\tilde{\mathbf{w}} = \mathbf{w} + \delta \tilde{\mathbf{w}}$, we

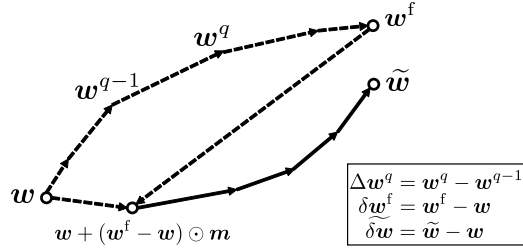


Figure 1: The figure depicts the overall approach that consists of two steps. The first step is depicted with dotted arrows and starts from the deployed network weights \mathbf{w} . In Q steps, the network is optimized which results in weights \mathbf{w}^f . Based on the collected information, a mask \mathbf{m} is determined that characterizes the set of weights that are rewound to the ones of \mathbf{w} . Therefore, the initial solution for the second step has weights $\mathbf{w} + \delta \mathbf{w}^f \odot \mathbf{m}$. This initial solution is further optimized to the new weights $\tilde{\mathbf{w}}$ by only changing weights that are allowed according to the mask, *i.e.*, $\delta \tilde{\mathbf{w}}$ has only nonzero elements where the mask is 1.

conduct a sparse fine-tuning, *i.e.*, we keep all weights with $m_i = 0$ constant during the optimization. Therefore, $\widetilde{\delta\mathbf{w}}$ is zero wherever $m_i = 0$, and only weights where $m_i = 1$ are updated.

3.1 Metrics for Rewinding

We will now describe a new metric that allows to determine the weights that should be kept constant, *i.e.*, those whose masks satisfy $m_i = 0$. The two-step approach relies on the following assumption: the better the loss $\ell(\mathbf{w} + \delta\mathbf{w}^f \odot \mathbf{m})$ of the initial solution for the second step, the better the final loss $\ell(\widetilde{\mathbf{w}})$. Therefore, the first step in the method should select a mask \mathbf{m} such that the loss difference $\ell(\mathbf{w} + \delta\mathbf{w}^f \odot \mathbf{m}) - \ell(\mathbf{w}^f)$ is as small as possible.

We will determine an optimized mask \mathbf{m} by combining two different view points. The ‘‘global contribution’’ uses information contained in the difference $\delta\mathbf{w}^f$ between the initial weights \mathbf{w} and the optimized weights \mathbf{w}^f by the first step. The ‘‘local contribution’’ takes into account some information that is gathered during the optimization in the first step, *i.e.*, in the path from \mathbf{w} to \mathbf{w}^f . Both kinds of information will be combined in order to determine an optimized mask \mathbf{m} .

The two view points are based on the concept of smooth differentiable functions, see for example [17]. A function $f(x)$ with $f : \mathbb{R}^d \rightarrow \mathbb{R}$ is called L -smooth if it has a Lipschitz continuous gradient $g(x)$: $\|g(x) - g(y)\|_2 \leq L\|x - y\|_2$ for all x, y . Note that Lipschitz continuity of a gradient is a stronger condition and is essential to ensuring convergence of many gradient-based algorithms. Under such a condition, one can derive the following bounds, see also [17]:

$$|f(y) - f(x) - g(x)^T \cdot (y - x)| \leq L/2 \cdot \|y - x\|_2^2 \quad \forall x, y \quad (4)$$

This basic relation is used to justify the global and the local contributions, *i.e.*, the rewinding metrics.

Global Contribution. Following some state-of-the-art methods for pruning, one would argue that a large absolute value in $\delta\mathbf{w}^f = \mathbf{w}^f - \mathbf{w}$ indicates that this weight has moved far from its initial value in \mathbf{w} . This reasoning leads to the widely used unstructured magnitude pruning, in order to solve the problem of determining an optimized mask \mathbf{m} . Magnitude pruning prunes the weights with the lowest magnitudes in a network, which is the current best-performed pruning method aiming at the trade-off between the model accuracy and the number of zero’s weights [21].

Based on Eq.(4), we can bound the relevant difference in the loss $\ell(\mathbf{w} + \delta\mathbf{w}^f \odot \mathbf{m}) - \ell(\mathbf{w}^f) \geq 0$ as

$$\ell(\mathbf{w} + \delta\mathbf{w}^f \odot \mathbf{m}) - \ell(\mathbf{w}^f) \leq g(\mathbf{w}^f)^T \cdot (\delta\mathbf{w}^f \odot (\mathbf{m} - \mathbf{1})) + L/2 \cdot \|\delta\mathbf{w}^f \odot (\mathbf{m} - \mathbf{1})\|_2^2 \quad (5)$$

where $g(\mathbf{w}^f)$ denotes the gradient of the loss function at \mathbf{w}^f , and $\mathbf{1}$ is a vector whose elements are all 1. As the loss is optimized at \mathbf{w}^f , we can assume that the gradient term is much smaller than the norm of the weight differences in Eq.(5). Therefore, we obtain approximately

$$\ell(\mathbf{w} + \delta\mathbf{w}^f \odot \mathbf{m}) - \ell(\mathbf{w}^f) \lesssim L/2 \cdot \|\delta\mathbf{w}^f \odot (\mathbf{1} - \mathbf{m})\|_2^2$$

The right hand side is clearly minimized if $m_i = 1$ for the largest absolute values of $\delta\mathbf{w}^f$. This information is captured in the contribution vector

$$\mathbf{c}^{\text{global}} = \delta\mathbf{w}^f \odot \delta\mathbf{w}^f \quad (6)$$

as $\mathbf{1}^T \cdot (\mathbf{c}^{\text{global}} \odot (\mathbf{1} - \mathbf{m})) = \|\delta\mathbf{w}^f \odot (\mathbf{1} - \mathbf{m})\|_2^2$.

In summary, the kI weights with the largest values in $\mathbf{c}^{\text{global}}$ are assigned to mask values $m_i = 1$ and are further fine-tuned in the second step, whereas all others are rewound from \mathbf{w}^f , and keep their initial values in \mathbf{w} . The pseudocode of Alg. 2 in Appendix A.1 shows this first approach.

Local Contribution. As experiments show, one can do better when using in addition some information gathered during the first step, *i.e.*, optimizing the initial weights \mathbf{w} in Q traditional optimization steps, $\mathbf{w} = \mathbf{w}^0 \rightarrow \dots \rightarrow \mathbf{w}^{q-1} \rightarrow \mathbf{w}^q \rightarrow \dots \rightarrow \mathbf{w}^Q = \mathbf{w}^f$. Again, starting from Eq.(4), we can derive bounds for each optimization step as

$$\ell(\mathbf{w}^{q-1}) - \ell(\mathbf{w}^q) \leq -g(\mathbf{w}^{q-1})^T \cdot \Delta\mathbf{w}^q + L/2 \cdot \|\Delta\mathbf{w}^q\|_2^2 \quad (7)$$

where $\Delta\mathbf{w}^q = \mathbf{w}^q - \mathbf{w}^{q-1}$. For a conventional gradient descent optimizer with a small learning rate we can use the approximation $|g(\mathbf{w}^{q-1})^T \cdot \Delta\mathbf{w}^q| \gg \|\Delta\mathbf{w}^q\|_2^2$ and obtain $\ell(\mathbf{w}^{q-1}) - \ell(\mathbf{w}^q) \leq$

$-g(w^{q-1})^T \cdot \Delta w^q$. Summing up over all optimization iterations yields approximately

$$\ell(w^f - \delta w^f) - \ell(w^f) \lesssim - \sum_{q=1}^Q g(w^{q-1})^T \cdot \Delta w^q \quad (8)$$

Note that we have $w = w^f - \delta w^f$ and $\delta w^f = \sum_{q=1}^Q \Delta w^q$. Therefore, with $m \sim 0$ we can reformulate Eq.(8) as $\ell(w + \delta w^f \odot m) - \ell(w^f) \lesssim U(m)$ with the upper bound $U(m) = - \sum_{q=1}^Q g(w^{q-1})^T \cdot (\Delta w^q \odot (\mathbf{1} - m))$ where we suppose that the gradients are approximately constant for small m . Therefore, an approximate incremental contribution of each weight dimension to the upper bound on the loss difference $\ell(w + \delta w^f \odot m) - \ell(w^f)$ can be determined as

$$c^{\text{local}} = - \frac{\partial U(m)}{\partial m} = - \sum_{q=1}^Q g(w^{q-1}) \odot \Delta w^q \quad (9)$$

This term is used to model the accumulated contribution of each weight to the overall loss reduction.

Combining Global and Local Contribution. So far, we independently calculate the global and local contributions c^{global} and c^{local} , respectively. It turns out experimentally, that a simple sum of both contributions leads to sufficiently good and robust final results, namely adding their normalized values. Therefore, the total contribution is computed as

$$c = \frac{1}{\mathbf{1}^T \cdot c^{\text{global}}} c^{\text{global}} + \frac{1}{\mathbf{1}^T \cdot c^{\text{local}}} c^{\text{local}}$$

and $m_i = 1$ for the kI largest values of c and $m_i = 0$ otherwise. The pseudocode of the corresponding algorithm is shown in Alg. 1.

Algorithm 1: Deep Partial Updating

Input: weights w , dataset \mathcal{D} , updating ratio k , learning rate $\{\alpha^q\}_{q=1}^Q$ in Q iterations

Output: weights \tilde{w}

/* The first step: full updating and rewinding */

Initiate $w^0 = w$;

Initiate $c^{\text{local}} = \mathbf{0}$;

for $q \leftarrow 1$ **to** Q **do**

Compute the loss gradient $g(w^{q-1}) = \frac{\partial \ell(w^{q-1})}{\partial w^{q-1}}$;
Compute the optimization step with learning rate α^q **as** Δw^q ;
Update $w^q = w^{q-1} + \Delta w^q$;
Update $c^{\text{local}} = c^{\text{local}} - g(w^{q-1}) \odot \Delta w^q$;

Get $w^f = w^Q$;

Compute the increment of weights $\delta w^f = w^f - w$;

Compute $c^{\text{global}} = \delta w^f \odot \delta w^f$;

Compute the combined contribution $c = c^{\text{global}} / (\mathbf{1}^T \cdot c^{\text{global}}) + c^{\text{local}} / (\mathbf{1}^T \cdot c^{\text{local}})$;

Sort the values in c **in descending order**;

Create a mask m **with 1 for the indices of Top- kI values in the above order, 0 for others**;

/* The second step: sparse fine-tuning */

Initiate $\tilde{\delta w} = \delta w^f \odot m$;

Initiate $\tilde{w} = w + \tilde{\delta w}$;

for $q \leftarrow 1$ **to** Q **do**

Compute the optimization step on \tilde{w} **with learning rate** α^q **as** $\Delta \tilde{w}^q$;
Update $\tilde{\delta w} = \tilde{\delta w} + \Delta \tilde{w}^q \odot m$ **and** $\tilde{w} = w + \tilde{\delta w}$;

3.2 Randomness of Initial Weights

In this section, we discuss the initialization of our method. \mathcal{D}^1 denotes the initial dataset used to train the network w^1 from a randomly initialized network w^0 . \mathcal{D}^1 corresponds to the available dataset

before deployment, or collected in the 0th round if there are no data available before deployment. $\{\delta\mathcal{D}^r\}_{r=2}^R$ denotes newly collected samples in each subsequent round.

To further improve the performance along a large number of rounds, we propose to reinsert some randomness in the initial weights of the first step after several rounds. We conducted experiments on full updating along the rounds, and compare the inference accuracy with a different initialization (see Appendix D.1). The results show that starting from a randomly initialized network can yield a higher accuracy after several rounds, in comparison to always start training from w^{r-1} of the last round. Therefore, we propose to add some new randomness into the network after a certain number of rounds. To maintain some randomness, w^1 is also partially updated from w^0 when training on \mathcal{D}^1 .

Specially, the network w^{r-1} is re-initialized after $1/k$ rounds, *i.e.*, Alg. 1 starts from a random network and then conducts the partial updating. The re-initialized random network can be sent to the edge devices through either a random seed if the devices have a random generator, or via the entire network once. In the following, we use Deep Partial Updating (DPU) to present rewinding according to the combined contribution to the loss reduction (*i.e.*, Alg. 1) with the above re-initialization.

4 Evaluation

We implement DPU with Pytorch [18], and evaluate its performance on multiple vision datasets, including MNIST [13], CIFAR10 [12], ILSVRC12 (ImageNet) [22] using multilayer perceptron (MLP), VGGNet [6, 20], ResNet34 [8], respectively. We randomly select 30% of each original test dataset (original validation dataset for ILSVRC12) as the validation dataset, and the remainder as the test dataset. Let $|\cdot|$ denote the number of samples in the dataset. Let $\{|\mathcal{D}^1|, |\delta\mathcal{D}^r|\}$ represent the available data samples along rounds, where $|\delta\mathcal{D}^r|$ is supposed to be constant along rounds. Both \mathcal{D}^1 and $\delta\mathcal{D}^r$ are randomly drawn from the original training dataset (only for evaluation purposes). For all pre-processing and random initialization, we apply the tools provided in Pytorch. We use the average cross-entropy as the loss function without a regularization term for better studying the effect on the training error caused by newly added data samples. We use Adam variant of SGD as the optimizer, except that Nesterov SGD is used for ResNet34 following the suggestions in [21]. The test accuracy is reported, when the validation dataset achieves the highest Top-1 accuracy. When the validation accuracy does not increase compared to the last round, the model will not be updated to reduce communication overhead. More implementation details are provided in the Appendix C. We will open-source the code upon acceptance.

One-shot Rewinding vs Iterative Rewinding. Based on previous experiments on pruning [21], iterative pruning with retraining may yield a higher accuracy compared to one-shot pruning, yet requiring several times more optimization iterations. This paper focuses on comparing the performance of DPU with other baselines including full updating given the same number of optimization iterations per round. Thus, we conduct one-shot rewinding at each round, *i.e.*, the rewinding is executed only once to achieve the desired sparsity (as shown in Alg. 1).

Indexing. DPU generates a sparse tensor. In addition to the updated weights, the indices of these weights also need to be sent to each edge device. A simple implementation is to send the mask \mathbf{m} . \mathbf{m} is a binary vector with I elements, which are assigned with 1 if the corresponding weights are updated. Let S_w denote the bitwidth of each single weight, and S_x denote the bitwidth of each index. Directly sending \mathbf{m} yields an overall communication cost of $I \cdot k \cdot S_w + I \cdot S_x$ with $S_x = 1$.

To save the communication cost on indexing, we further encode \mathbf{m} . Suppose that \mathbf{m} is a random binary vector with a probability of k to contain 1. The optimal encoding scheme according to Shannon yields $S_x(k) = k \cdot \log(1/k) + (1 - k) \cdot \log(1/(1 - k))$. Coding schemes such as Huffman block coding can come close to this bound. Partial updating results in a smaller communication data size than full updating, if $S_w \cdot I > S_w \cdot k \cdot I + S_x(k) \cdot I$. Under the worst case for indexing cost, *i.e.*, $S_x(k = 0.5) = 1$, as long as $k < (32 - 1)/32 = 0.97$, partial updating can yield a smaller communication data size with $S_w = 32$ -bit weights. In the following experiments, we will use $S_w \cdot k \cdot I + S_x(k) \cdot I$ to report the size of data transmitted from server to each node at each round, contributed by the partially updated weights plus the encoded indices of these weights.

4.1 Ablation Study of Metrics

Settings. We first conduct a set of ablation experiments regarding different metrics of rewinding discussed in Sec. 3.1. We compare the influence of the local and global contributions as well as their combination, in terms of the incremental training loss caused by rewinding. The original VGGNet and ResNet34 are fully trained on a randomly selected dataset of 10^3 and 4×10^5 samples, respectively. We execute full updating, *i.e.*, the first step of our approach, after adding 10^3 and 2×10^5 new randomly selected samples, respectively. Afterwards, we conduct one-shot rewinding with all three metrics, *i.e.*, global contribution, local contribution, and combined contribution. Each experiment is conducted for one round. We report the results over five runs.

Results. The training loss (mean \pm standard deviation) after full updating (*i.e.*, $\ell(\mathbf{w}^f)$) and after rewinding (*i.e.*, $\ell(\mathbf{w} + \delta\mathbf{w}^f \odot \mathbf{m})$) with three metrics is reported in Table 1. As seen in the table, the combined contribution always yields a lower or similar training loss after rewinding compared to the other two metrics. The smaller deviation also indicates that adopting the combined contribution yields more robust results. This validates the effectiveness of our proposed metric, *i.e.*, the combined contribution to the analytical upper bound on loss reduction.

Table 1: Comparing the training loss after rewinding according to different metrics.

| Benchmark | k | Training loss | | | |
|------------------------|-------------------|-------------------|-------------------|-------------------------------------|-------------------------------------|
| | | Full updating | Global | Local | Combined |
| VGGNet (CIFAR10) | 0.01 | | 3.042 ± 0.068 | 2.588 ± 0.084 | 2.658 ± 0.086 |
| | 0.05 | 0.086 ± 0.001 | 2.509 ± 0.056 | 1.799 ± 0.104 | 1.671 ± 0.062 |
| | 0.1 | | 2.031 ± 0.046 | 1.337 ± 0.076 | 0.994 ± 0.034 |
| | 0.2 | | 1.196 ± 0.049 | 0.739 ± 0.031 | 0.417 ± 0.009 |
| 0.01 | 3.340 ± 0.109 | | 4.222 ± 0.156 | 3.179 ± 0.052 | |
| ResNet34 (ILSVRC12) | 0.05 | 1.016 ± 0.000 | 2.005 ± 0.064 | 2.346 ± 0.036 | 1.844 ± 0.022 |
| | 0.1 | | 1.632 ± 0.044 | 2.662 ± 0.048 | 1.609 ± 0.025 |
| | 0.2 | | 1.331 ± 0.016 | 3.626 ± 0.062 | 1.327 ± 0.008 |

4.2 Evaluation on Different Benchmarks

Settings. We compare DPU to three baseline methods, including (i) full updating (FU), where at each round the network is fully updated with a random initialization (*i.e.*, training from scratch, which yields a better performance as discussed in Sec. 3.2); (ii) random partial updating (RPU), where the network is trained from \mathbf{w}^{r-1} , while we randomly fix each layer’s weights with a ratio of $(1 - k)$ and sparsely fine-tune the rest; and (iii) global contribution partial updating (GCPU), where the network is trained with Alg. 2 without re-initialization described in Sec. 3.2. The experiments are conducted with different types of networks on different benchmarks as mentioned earlier.

Results. We plot results in terms of test accuracy in Fig. 2. As seen in this figure, DPU clearly yields the highest accuracy in comparison to the other partial updating schemes on different benchmarks. For example, DPU can yield a final Top-1 accuracy of 93.25% on VGGNet, even exceeds the accuracy (92.46%) of full updating, while GCPU and RPU only acquire 90.67% and 88.31% respectively. In addition, we compare three partial updating schemes in terms of the accuracy difference related to full updating averaged over all rounds, and the ratio of the communication cost over all rounds related to full updating in Table 2. As seen in the table, DPU reaches a similar or even higher accuracy as full updating, while incurring significantly fewer transmitted data sent from the server to each edge node. Specially, DPU saves around 99.6%, 93.8% and 77.7% of transmitted data on MLP, VGGNet, and ResNet34, respectively (90.4% in average).

We further investigate the benefit due to DPU in terms of the total communication cost reduction, as DPU has no impact on the edge-to-server communication involving newly collected data samples. This experimental setup assumes that all data samples in $\delta\mathcal{D}^r$ are collected by N edge nodes during all rounds and sent to the server on a per-round basis. For clarity, let S_d denote the data size of each training sample. During round r , we define per-node communication cost under DPU as $S_d \cdot |\delta\mathcal{D}^r|/N + (S_w \cdot k \cdot I + S_x(k) \cdot I)$. Due to space constraints, the detailed results are shown in Appendix D.2. We observe that DPU can still achieve a significant reduction on the total

communication cost, *e.g.*, reducing up to 87% on updating MLP and VGGNet even for the worst case (*i.e.*, a single node). Moreover, DPU tends to be more beneficial when the size of data transmitted by each node to the server becomes smaller. This is intuitive because in this case the server-to-edge communication cost (thus the reduction due to DPU) dominates in the entire communication cost.

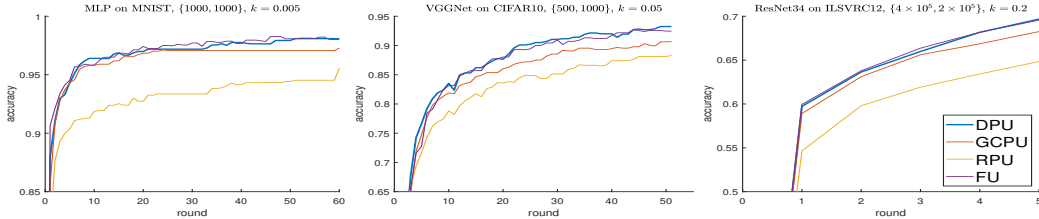


Figure 2: DPU is compared with other baselines on different benchmarks in terms of the test accuracy.

Table 2: The average accuracy difference over all rounds and the ratio of communication cost over all rounds related to full updating.

| Method | Average accuracy difference | | | Ratio of communication cost | | |
|--------|-----------------------------|--------|----------|-----------------------------|--------|----------|
| | MLP | VGGNet | ResNet34 | MLP | VGGNet | ResNet34 |
| DPU | -0.22% | +0.54% | -0.12% | 0.0042 | 0.0624 | 0.2226 |
| GCPU | -0.74% | -1.63% | -1.01% | 0.0033 | 0.0640 | 0.2226 |
| RPU | -4.06% | -4.09% | -4.64% | 0.0055 | 0.0606 | 0.2226 |

4.3 Impact due to Varying Number of Data Samples and Updating Ratios

Settings. In this set of experiments, we demonstrate that DPU outperforms other baselines under varying number of data samples and updating ratios. We also conduct an ablation study concerning the randomness of the initial weights, *i.e.*, re-initialization in Sec. 3.2. We implement DPU with and without re-initialization, GCPU with and without re-initialization and RPU (see Sec. 4.2) on VGGNet using CIFAR10 dataset. We compare these methods with different amounts of training samples $\{|\mathcal{D}^1|, |\delta\mathcal{D}^r|\}$ and different updating ratios. Each experiment runs three times using random data samples.

Results. We compare the difference between the accuracy under each partial updating method and that under full updating. The mean accuracy difference (over three runs) is plotted in Fig. 3. A comprehensive set of results including the standard deviations of the accuracy difference is provided in Appendix D.3. As seen in Fig. 3, DPU with re-initialization achieves the highest accuracy in all scenarios. The dashed curves and the solid curves with the same color can be viewed as the ablation study of re-initialization. Re-initialization provides the optimizer of the first step a higher probability to jump out of a local optima, which may result in a better-performing partial updating. Particularly given a large number of rounds, it is critical to add randomness to the start point w^{r-1} after performing several rounds (as discussed in Sec. 3.2).

5 Conclusion

In this paper, we present the weight-wise deep partial updating paradigm, motivated by the fact that full weight updating may be impossible in many edge intelligence scenarios. We present DPU, which is established through analytically upper-bounding the loss difference between partial updating and full updating, and only updating the weights which make the largest contributions to the upper bound. Extensive experimental results demonstrate the efficacy of DPU which achieves a high inference accuracy while updating a rather small number of weights.

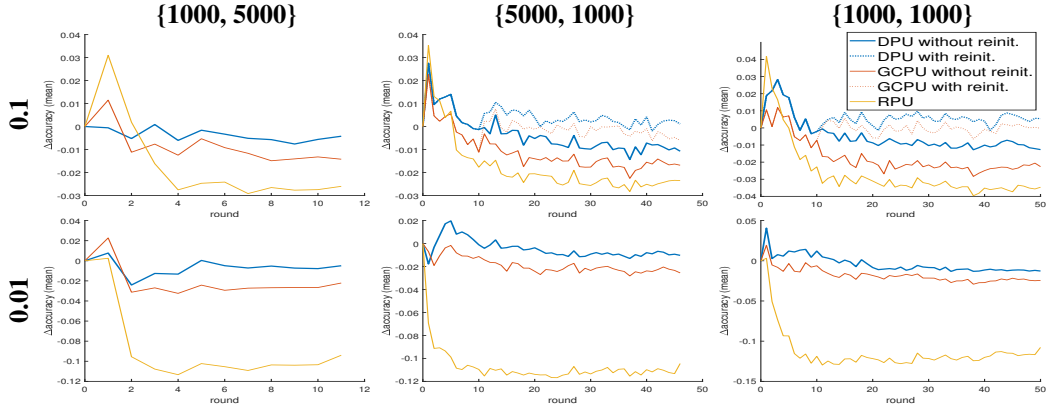


Figure 3: Comparison w.r.t. accuracy difference under different $\{|\mathcal{D}^1|, |\delta\mathcal{D}^r|\}$ and updating ratio (0.1 and 0.01) settings.

Broader Impact

Our proposed DPU establishes the weight-wise deep partial updating paradigm, which enables complex DNN models to be deployed and updated efficiently for edge intelligence systems. The key benefit is to allow the server to retrain the model by updating only a partial set of the model weights while maintaining similar performance as if a full weight updating were performed. Transmitting only a subset of the weights which are updated from server to each edge device significantly reduces the communication cost. DPU can be applied to many important application domains which greatly benefit our society, including vision robotic sensing in an unknown environment, local translators on mobile phones, and acoustic sensor networks deployed in Alpine environments. Without partial updating, powerful yet complex DNN model design is unlikely to impact such edge intelligence systems. We believe DPU could be a key enabler for DNN-driven edge computing systems where the edge device’s capability in terms of communication and computation is rather limited (*e.g.*, sensors and internet-of-things devices).

References

- [1] Jordan T. Ash, Chicheng Zhang, Akshay Krishnamurthy, John Langford, and Alekh Agarwal. Deep batch active learning by diverse, uncertain gradient lower bounds. In *International Conference on Learning Representations*, 2020.
- [2] Aishwarya Bhandare, Vamsi Sripathi, Deepthi Karkada, Vivek Menon, Sun Choi, Kushal Datta, and Vikram Saleatore. Efficient 8-bit quantization of transformer neural machine language translation model. In *Proceedings of the 34th International Conference on Machine Learning, Joint Workshop on On-Device Machine Learning & Compact Deep Neural Network Representations*, 2019.
- [3] S Brown and CJ Sreenan. Updating software in wireless sensor networks: A survey. *Dept. of Computer Science, National Univ. of Ireland, Maynooth, Tech. Rep.*, pages 1–14, 2006.
- [4] Niladri Chatterji, Behnam Neyshabur, and Hanie Sedghi. The intriguing role of module criticality in the generalization of deep networks. In *International Conference on Learning Representations*, 2020.
- [5] Yunjey Choi. Pytorch tutorial on language model. https://github.com/yunjey/pytorch-tutorial/tree/master/tutorials/02-intermediate/language_model. Accessed: 2020-03-17.
- [6] Matthieu Courbariaux, Yoshua Bengio, and Jean-Pierre David. Binaryconnect: Training deep neural networks with binary weights during propagations. In *Proceedings of Advances in Neural Information Processing Systems*, pages 3123–3131, 2015.

- [7] Song Han, Huizi Mao, and William J Dally. Deep compression: Compressing deep neural networks with pruning, trained quantization and huffman coding. In *Proceedings of International Conference on Learning Representations*, 2016.
- [8] Kaiming He, Xiangyu Zhang, Shaoqing Ren, and Jian Sun. Deep residual learning for image recognition. In *Proceedings of IEEE Conference on Computer Vision and Pattern Recognition*, 2016.
- [9] Sepp Hochreiter and Jürgen Schmidhuber. Long short-term memory. *Neural computation*, 9(8):1735–1780, 1997.
- [10] Mark Horowitz. 1.1 computing’s energy problem (and what we can do about it). In *2014 IEEE International Solid-State Circuits Conference Digest of Technical Papers (ISSCC)*, 2014.
- [11] Sangwon Jung, Hongjoon Ahn, Sungmin Cha, and Taesup Moon. Adaptive group sparse regularization for continual learning. *CoRR*, 2020.
- [12] Alex Krizhevsky, Vinod Nair, and Geoffrey Hinton. Cifar10 (canadian institute for advanced research). <http://www.cs.toronto.edu/~kriz/cifar.html>.
- [13] Yann LeCun and Corinna Cortes. MNIST handwritten digit database. <http://yann.lecun.com/exdb/mnist/>, 2010.
- [14] Mitchell P Marcus, Mary Ann Marcinkiewicz, and Beatrice Santorini. Building a large annotated corpus of english: The penn treebank. *Computational Linguistics*, 19(2):313–330, 1993.
- [15] Z. Meng, H. Qin, Z. Chen, X. Chen, H. Sun, F. Lin, and M. H. Ang. A two-stage optimized next-view planning framework for 3-d unknown environment exploration, and structural reconstruction. *IEEE Robotics and Automation Letters*, 2(3):1680–1687, 2017.
- [16] Matthias Meyer, Timo Farei-Campagna, Akos Pasztor, Reto Da Forno, Tonio Gsell, Jérôme Faillettaz, Andreas Vieli, Samuel Weber, Jan Beutel, and Lothar Thiele. Event-triggered natural hazard monitoring with convolutional neural networks on the edge. In *Proceedings of the 18th International Conference on Information Processing in Sensor Networks, IPSN ’19*. Association for Computing Machinery, 2019.
- [17] Yurii Nesterov. Introductory lectures on convex programming volume i: Basic course. *Lecture notes*, 1:25, 1998.
- [18] Adam Paszke, Sam Gross, Soumith Chintala, Gregory Chanan, Edward Yang, Zachary DeVito, Zeming Lin, Alban Desmaison, Luca Antiga, and Adam Lerer. Automatic differentiation in pytorch. In *Proceedings of NIPS Autodiff Workshop: The Future of Gradient-based Machine Learning Software and Techniques*, 2017.
- [19] Pytorch. Pytorch example on resnet. <https://github.com/pytorch/vision/blob/master/torchvision/models/resnet.py>. Accessed: 2019-10-15.
- [20] Mohammad Rastegari, Vicente Ordonez, Joseph Redmon, and Ali Farhadi. Xnor-net: Imagenet classification using binary convolutional neural networks. In *Proceedings of European Conference on Computer Vision*, pages 525–542, 2016.
- [21] Alex Renda, Jonathan Frankle, and Michael Carbin. Comparing fine-tuning and rewinding in neural network pruning. In *International Conference on Learning Representations*, 2020.
- [22] Olga Russakovsky, Jia Deng, Hao Su, Jonathan Krause, Sanjeev Satheesh, Sean Ma, Zhiheng Huang, Andrej Karpathy, Aditya Khosla, Michael Bernstein, Alexander C. Berg, and Li Fei-Fei. Imagenet large scale visual recognition challenge. *International Journal of Computer Vision*, 115(3):211–252, 2015.
- [23] Reza Shokri and Vitaly Shmatikov. Privacy-preserving deep learning. In *Proceedings of the 22nd ACM SIGSAC Conference on Computer and Communications Security, CCS ’15*, 2015.
- [24] Karen Simonyan and Andrew Zisserman. Very deep convolutional networks for large-scale image recognition. In *Proceedings of International Conference on Learning Representations*, 2015.
- [25] Samarth Sinha, Sayna Ebrahimi, and Trevor Darrell. Variational adversarial active learning. In *IEEE International Conference on Computer Vision*, 2019.
- [26] Jaehong Yoon, Eunho Yang, Jeongtae Lee, and Sung Ju Hwang. Lifelong learning with dynamically expandable networks. In *International Conference on Learning Representations*, 2018.

Appendix

A Pseudocodes

A.1 Global Contribution Partial Updating

The magnitude pruning method prunes (*i.e.*, set as zero) weights with the lowest magnitudes in a network, which is the current best-performed pruning method aiming at the trade-off between the model accuracy and the number of zero’s weights [21]. We adapt the magnitude pruning proposed in [21] to prune the incremental weights δw^f . Specially, the elements with the smallest absolute values in δw^f are set to zero (also rewinding), while the remaining weights are further sparsely fine-tuned with the same learning rate schedule as training w^f .

Algorithm 2: Global Contribution Partial Updating (Prune Incremental Weights)

Input: weights w , dataset \mathcal{D} , updating ratio k , learning rate $\{\alpha^q\}_{q=1}^Q$ in Q iterations
Output: weights \tilde{w}
 /* The first step: full updating and rewinding (pruning) */
Initiate $w^0 = w$;
for $q \leftarrow 1$ to Q **do**
 Compute the loss gradient $g(w^{q-1}) = \frac{\partial \ell(w^{q-1})}{\partial w^{q-1}}$;
 Compute the optimization step with learning rate α^q **as** Δw^q ;
 Update $w^q = w^{q-1} + \Delta w^q$;
Get $w^f = w^Q$;
Compute the increment of weights $\delta w^f = w^f - w$;
Compute $c^{\text{global}} = \delta w^f \odot \delta w^f$;
Sort the values in c^{global} **in descending order**;
Create a mask m **with 1 for the indices of Top- kI values in the above order, 0 for others**;
 /* The second step: sparse fine-tuning */
Initiate $\tilde{\delta w} = \delta w^f \odot m$;
Initiate $\tilde{w} = w + \tilde{\delta w}$;
for $q \leftarrow 1$ to Q **do**
 Compute the optimization step on \tilde{w} **with learning rate** α^q **as** $\Delta \tilde{w}^q$;
 Update $\tilde{\delta w} = \tilde{\delta w} + \Delta \tilde{w}^q \odot m$ **and** $\tilde{w} = w + \tilde{\delta w}$;

In comparison to traditional pruning on weights, pruning on incremental weights has a different start point. Traditional pruning on weights first trains randomly initialized weights (a zero-initialized network cannot be trained due to the symmetry), and then prunes the weights with the smallest magnitudes. However, the increment of weights δw^f is initialized with zero in Alg. 2, since the first step starts from w . This implies that pruning δw^f has the same functionality as rewinding these weights to their initial values in w .

B Complexity Analysis

Algorithm 1: Deep Partial Updating. Recall that the dimensionality of the weights vector is denoted as I . In Q optimization iterations during the first step, Alg. 1 introduces an extra time complexity of $O(QI)$, and an extra space complexity of $O(I)$ related to the original optimizer. The rest of the first step takes a time complexity of $O(I \cdot \log(I))$ and a space complexity of $O(I)$, (*e.g.*, using heap sort or quick sort). In Q optimization iterations during the second step, Alg. 1 introduces an extra time complexity of $O(QI)$, and an extra space complexity of $O(I)$ related to the original optimizer. Thus, a total extra time complexity is $O(2QI + I \cdot \log(I))$ and a total extra space complexity is $O(I)$.

Algorithm 2: Global Contribution Partial Updating. In Q optimization iterations during the first step, Alg. 2 does not introduce extra time complexity or extra space complexity related to the original

optimizer. The rest of the first step takes a time complexity of $O(I \cdot \log(I))$ and a space complexity of $O(I)$, (e.g., using heap sort or quick sort). In Q optimization iterations during the second step, Alg. 2 introduces an extra time complexity of $O(QI)$, and an extra space complexity of $O(I)$ related to the original optimizer. Thus, a total extra time complexity is $O(QI + I \cdot \log(I))$ and a total extra space complexity is $O(I)$.

C Implementation Details

C.1 MLP on MNIST

The MNIST dataset [13] consists of 28×28 gray scale images in 10 digit classes. It contains a training dataset with 60000 data samples, and a test dataset with 10000 data samples. We use the original training dataset for training; and randomly select 3000 samples in the original test dataset for validation, and the rest 7000 samples for testing. We use a mini-batch with size of 128 training on 1 TITAN Xp GPU. We use Adam variant of SGD as the optimizer, and use all default parameters provided by Pytorch. The number of training epochs is chosen as 30, *i.e.*, in the r^{th} round, $Q = |\mathcal{D}^r|/128 \times 30$. The initial learning rate is 0.005, and it decays with a factor of 0.1 every 10 epochs. For fair comparison, we adopt the same learning rate for other baseline methods. Specially, for full updating (FU) and random partial updating (RPU), the network is fully updated and sparsely fine-tuned in $2Q$ iterations, respectively. The corresponding learning rate schedule used in DPU is also proportionally expanded for that used in full updating and random partial updating. That is, the initial learning rate is 0.005, and it decays with a factor of 0.1 for every 20 epochs. This setting is also used in the following experiments. The used MLP contains two hidden layers, and each hidden layer contains 512 hidden units. The input is a 784-dim tensor of all pixel values for each image. We use ReLU as the activation function, and use a softmax function as the non-linearity of the last layer (*i.e.*, the output layer) in the entire paper. All weights in MLP need around 2.67MB. Each data sample needs 0.784KB. The used MLP architecture is presented as, $2 \times 512\text{FC} - 10\text{SVM}$.

C.2 VGGNet on CIFAR10

The CIFAR10 dataset [12] consists of 32×32 color images in 10 object classes. It contains a training dataset with 50000 data samples, and a test dataset with 10000 data samples. We use the original training dataset for training; and randomly select 3000 samples in the original test dataset for validation, and the rest 7000 samples for testing. We use a mini-batch with size of 128 training on 1 TITAN Xp GPU. We use Adam variant of SGD as the optimizer, and use all default parameters provided by Pytorch. The number of training epochs is chosen as 30, *i.e.*, in the r^{th} round, $Q = |\mathcal{D}^r|/128 \times 30$. The initial learning rate is 0.005, and it decays with a factor of 0.2 every 10 epochs. The used VGGNet is widely adopted in many previous compression works [6, 20], which is a modified version of the original VGG [24]. All weights in VGGNet need around 56.09MB. Each data sample needs 3.072KB. The used VGGNet architecture is presented as, $2 \times 128\text{C3} - \text{MP2} - 2 \times 256\text{C3} - \text{MP2} - 2 \times 512\text{C3} - \text{MP2} - 2 \times 1024\text{FC} - 10\text{SVM}$.

C.3 ResNet34 on ILSVRC12

The ILSVRC12 (ImageNet) dataset [22] consists of high-resolution color images in 1000 object classes. It contains a training dataset with 1.2 million data samples, and a validation dataset with 50000 data samples. Following the commonly used pre-processing [19], each sample (single image) is randomly resized and cropped into a 224×224 color image. We use the original training dataset for training; and randomly select 15000 samples in the original validation dataset for validation, and the rest 35000 samples for testing. We use a mini-batch with size of 512 training on 4 TITAN Xp GPUs. According to the suggestions in [21], we use Nesterov SGD as the optimizer. We also use the parameters provided by [21] to configure Nesterov SGD optimizer. The number of training epochs is chosen as 45, *i.e.*, in the r^{th} round, $Q = |\mathcal{D}^r|/512 \times 45$. Thus, the number of training epochs for full updating is 90 as in [21]. The learning rate schedule in [21] is shrunk proportionally to fit in 45 epochs. We observe that ResNet34 on ILSVRC12 is more sensitive to the randomness of initial weights. Thus, we re-initialize the network once before the partial updating at the third round of DPU. The ResNet34 used in our experiments is proposed in [8]. All weights in ResNet34 need around

87.12MB. Each data sample needs 150.528KB. The network architecture is the same as “resnet34” in [19].

C.4 LSTM on Penn Treebank

We conduct partial updating on the word-level language modeling task to study the performance of DPU on recurrent neural network architectures. We use one of the most well-known recurrent neural networks, *i.e.*, long short-term memory (LSTM) [9]. We choose Penn Treebank (PTB) corpus [14] as the evaluation benchmark. The PTB dataset contains 929K training tokens, 73K validation tokens, and 82K testing tokens, where one token corresponds to one word. We still use the average cross-entropy as the loss function, and use Adam variant of SGD as the optimizer with a clipping on the gradient norm at 0.5 [5]. Since language modeling aims at predicting the next word, the performance is measured by perplexity per word (PPW) metric. The lower the perplexity, the higher the model performance. The test perplexity is reported, when the validation dataset achieves the lowest perplexity.

We mainly follow all settings in [5]. We use the standard pre-processing splits with a 10K size vocabulary. The file content is tokenized with a mini-batch size of 20, *i.e.*, the file is sequentially and uniformly split into 20 arrays. Since the tokenized file is constructed sequentially, both \mathcal{D}^1 and $\delta\mathcal{D}^r$ are cropped from 20 arrays sequentially, with $|\mathcal{D}^1|$ and $|\delta\mathcal{D}^r|$ tokens from each of 20 arrays respectively (only for evaluation purposes). The newly collected $\delta\mathcal{D}^r$ is also sequentially concatenated with the previous dataset to build the new training dataset at each round. For example, $\mathcal{D}^2 = \mathcal{D}^1 \cup \delta\mathcal{D}^2$, the total number of tokens contained in \mathcal{D}^2 is $|\mathcal{D}^2| \times 20 = (|\mathcal{D}^1| + |\delta\mathcal{D}^2|) \times 20$. Let $\{|\mathcal{D}^1|, |\delta\mathcal{D}^r|\}$ represent the available data samples along rounds, where $|\delta\mathcal{D}^r|$ is supposed to be constant along rounds. In this case, each data sample corresponds to 20 tokens (words). We use a fixed learning rate of 0.002. The used LSTM is also the same as [5], which contains 1 hidden layer of size 1024 and an embedding layer of size 128. We unroll the network for 30 time steps, *i.e.*, the sequence length is 30. The number of training epochs is chosen as 5 according to [5], *i.e.*, in the r^{th} round, $Q = (\text{ceil}(|\mathcal{D}^r|/30) - 1) \times 5$. All weights in LSTM need around 64.95MB. Since each English word contains 5 characters in average, each data sample (20 words) needs around 120 characters including the space, *i.e.*, 0.120KB in ASCII format.

D More Results

D.1 Full Updating

Settings. In this experiment, we compare full updating with a different initialization at each round in terms of the test accuracy. The compared full updating methods include, (i) the network is trained from a random initialization at each round; (ii) the network is trained from a same random initialization at each round, *i.e.*, with a same random seed; (iii) the network is trained from the weights w^{r-1} of the last round at each round. For fair comparison, all methods are trained with the same learning rate schedule and the same number of training iterations per round. Since training from a random initialization (*i.e.*, training from scratch) always requires more iterations (epochs) than training from the last round, the number of training iterations is selected to ensure all methods can be fully optimized within these iterations. The corresponding number of training iterations used at each round is set to $2Q$. The experiments are conducted on VGGNet using CIFAR10 dataset with different amounts of training samples $\{|\mathcal{D}^1|, |\delta\mathcal{D}^r|\}$. Each experiment runs for three times using random data samples and different random seeds.

Results. We report the mean and the standard deviation of test accuracy (over three runs) under different initialization in Fig. 4. The results show that training from a same random initialization yields a similar accuracy level while sometimes also a lower variance, as training from a (different) random initialization at each round. In comparison to training from scratch (*i.e.*, random initialization), training from w^{r-1} may yield a higher accuracy in the first few rounds; yet training from scratch may always outperform after a large number of rounds. Thus, in this paper, we adopt training from a same random initialization at each round, *i.e.*, (ii), as the baseline of full updating.

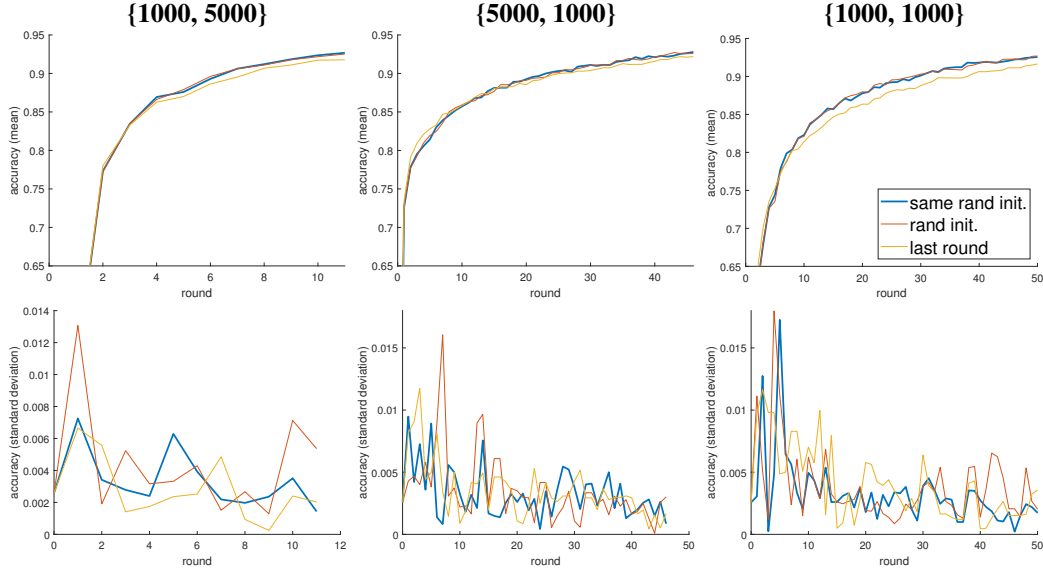


Figure 4: Comparing full updating methods with a different initialization at each round.

D.2 Evaluation on Different Benchmarks

D.2.1 Experiments on Total Communication Cost Reduction

Settings. In this experiment, we show the advantages of DPU in terms of the total communication cost reduction, as DPU has no impact on the edge-to-server communication which may involve sending newly collected data samples on nodes. The total communication cost includes both edge-to-server communication and server-to-edge communication. Here we assume that all samples in $\delta\mathcal{D}^r$ are collected by N edge nodes during all rounds and sent to the server on a per-round basis. For clarity, let S_d denote the data size of each training sample. During round r , we define the per-node total communication cost under DPU as $S_d \cdot |\delta\mathcal{D}^r|/N + (S_w \cdot k \cdot I + S_x(k) \cdot I)$. Similarly, the per-node total communication cost under full updating is defined as $S_d \cdot |\delta\mathcal{D}^r|/N + S_w \cdot I$.

In order to simplify the demonstration, we consider the scenario where N nodes send a certain amount of data samples to the server in $R - 1$ rounds, namely $\sum_{r=2}^R |\delta\mathcal{D}^r|$ (see Sec. 3.2). Thus, the average data size transmitted from each node to the server in all rounds is $\sum_{r=2}^R S_d \cdot |\delta\mathcal{D}^r|/N$. A larger N implies a fewer amount of transmitted data from each node to the server.

Results. We report the ratio of the total communication cost over all rounds required by DPU related to full updating, when DPU achieves a similar accuracy level as full updating (corresponding to three evaluations in Fig. 2). The ratio clearly depends on $\sum_{r=2}^R S_d \cdot |\delta\mathcal{D}^r|/N$, *i.e.*, the number of nodes N . The relation between the ratio and N is plotted in Fig. 5.

DPU can reduce up to 87% of the total communication cost on updating MLP and VGGNet even for only a single node. Single node corresponds to the largest data size during edge-to-server transmission per node, *i.e.*, the worst case. Moreover, DPU tends to be more beneficial when the size of data transmitted by each node to the server becomes smaller. This is intuitive because in this case the server-to-edge communication cost (thus the reduction due to DPU) dominates in the entire communication cost. For tasks with a large S_d , DPU can still significantly save the total communication cost with a large number of nodes (*e.g.*, some mobile applications). For example, partial updating ResNet34 on ILSVRC12 can save over 50% of the total communication cost in a 500-node sensing system.

D.2.2 LSTM on Penn Treebank

Settings. Similar as Sec. 4.2, we also compare DPU to three baseline methods on LSTM using Penn Treebank dataset, including (i) full updating (FU), where at each round the network is fully updated

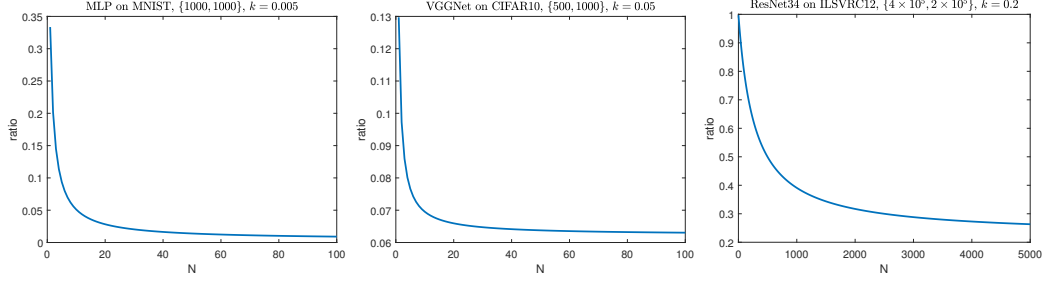


Figure 5: The ratio, between the total communication cost (over all rounds) under DPU and that under full updating, varies with the number of nodes N .

with a random initialization; (ii) random partial updating (RPU), where the network is trained from w^{r-1} , while we randomly fix each layer’s weights with a ratio of $(1 - k)$ and sparsely fine-tune the rest; and (iii) global contribution partial updating (GCPU), where the network is trained with Alg. 2 without re-initialization described in Sec. 3.2. We conduct the experiment under three updating ratios, 0.005, 0.01, and 0.05.

Results. We plot results in terms of test perplexity in Fig. 6. As seen in this figure, DPU clearly yields the lowest perplexity in comparison to the other partial updating schemes on LSTM. Similar as Sec. 4.2, we compare three partial updating schemes in terms of the perplexity difference related to full updating averaged over all rounds, as well as the ratio of the communication cost (server-to-edge) over all rounds related to full updating. We report the results under updating ratio $k = 0.05$ in Table 3. As seen in the table, DPU reaches a similar perplexity as full updating, while incurring significantly fewer transmitted data sent from the server to each edge node. In addition, we also report the ratio of the total communication cost (including edge-to-server and server-to-edge) over all rounds required by DPU related to full updating in Fig. 7. Note that text data samples require a relatively smaller data size compared to image data samples. As seen in this figure, DPU always achieves a significant reduction on the total communication cost (*e.g.*, 94% reduction even for the most pessimistic scenario, *i.e.*, $N = 1$).

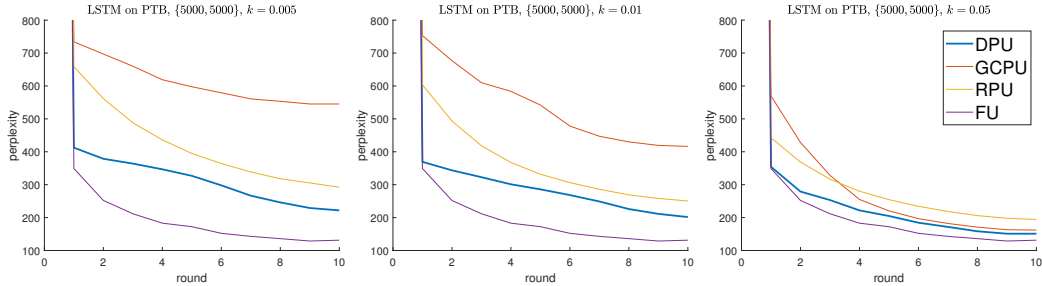


Figure 6: DPU is compared with other baselines on LSTM using PTB dataset in terms of the test perplexity.

Table 3: The average perplexity difference over all rounds and the ratio of communication cost (server-to-edge) over all rounds related to full updating (with $k = 0.05$).

| Method | Average perplexity difference | Ratio of communication cost |
|--------|-------------------------------|-----------------------------|
| DPU | +27.0 | 0.0531 |
| GCPU | +81.7 | 0.0589 |
| RPU | +85.4 | 0.0589 |

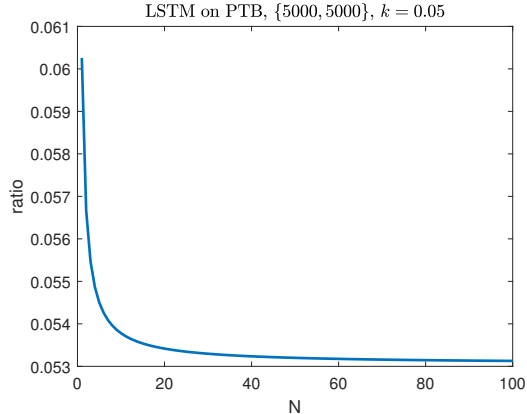


Figure 7: The ratio, between the total communication cost (over all rounds) under DPU and that under full updating, varies with the number of nodes N .

D.3 Impact due to Varying Number of Data Samples and Updating Ratios

Settings. In this set of experiments, we demonstrate that DPU outperforms other baselines under varying number of data samples and updating ratios. We also conduct an ablation study concerning the randomness of the initial weights, *i.e.*, re-initialization in Sec. 3.2. We implement DPU with and without re-initialization, GCPU with and without re-initialization and RPU (see Sec. 4.2) on VGGNet using CIFAR10 dataset. We compare these methods with different amounts of training samples $\{|\mathcal{D}^1|, |\delta\mathcal{D}^r|\}$ and different updating ratios. Each experiment runs three times using random data samples.

Results. We compare the difference between the accuracy under each partial updating method and that under full updating. The mean accuracy difference (over three runs) is plotted in Fig. 8. The standard deviation of the accuracy difference (over three runs) is provided in Fig. 9. As seen in Fig. 8, DPU with re-initialization achieves the highest accuracy in all scenarios. In addition, we also plot the mean and standard deviation of test accuracy (over three runs) of these methods (including full updating) in Fig. 10 and Fig. 11, respectively. The dashed curves and the solid curves with the same color can be viewed as the ablation study of re-initialization. Re-initialization always results in a better-performing partial updating than the ones without re-initialization. Particularly given a large number of rounds, it is critical to add randomness to the start point w^{r-1} after performing several rounds (as discussed in Sec. 3.2).

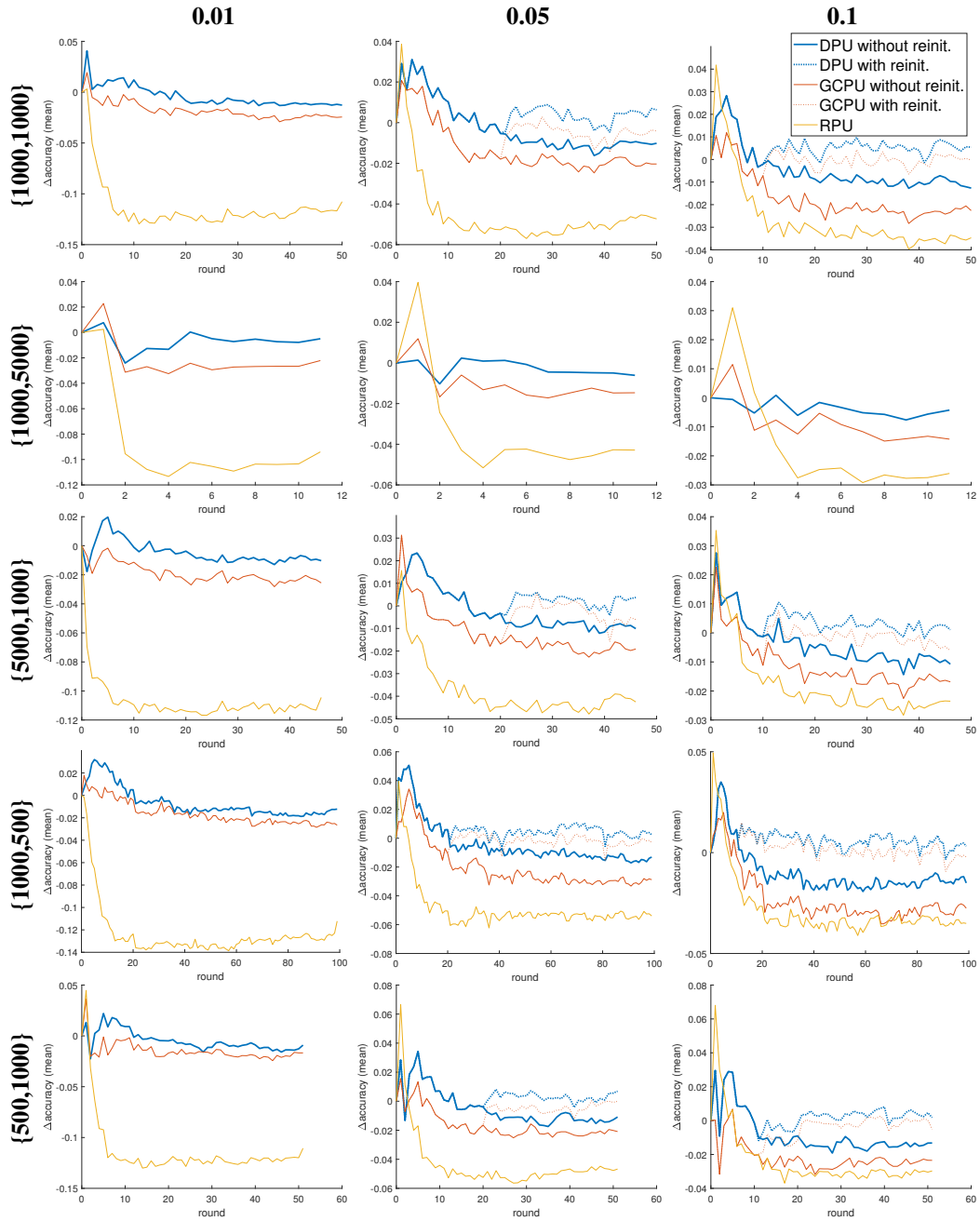


Figure 8: Comparison w.r.t. the mean accuracy difference under different $\{|\mathcal{D}^1|, |\delta\mathcal{D}^r|\}$ and updating ratio (0.01, 0.05 and 0.1) settings.

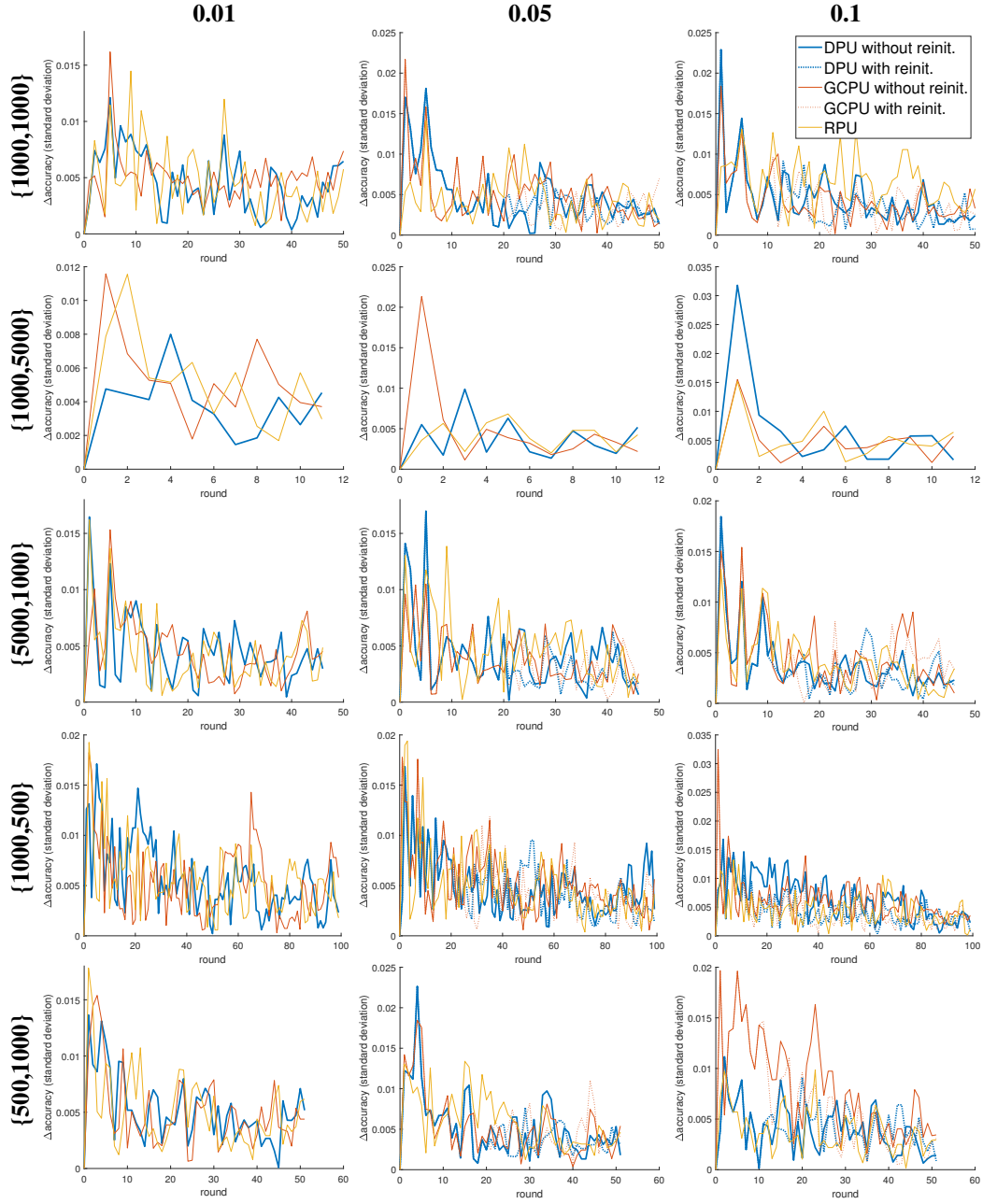


Figure 9: Comparison w.r.t. the standard deviation of accuracy difference under different $\{|\mathcal{D}^1|, |\delta\mathcal{D}^r|\}$ and updating ratio (0.01, 0.05 and 0.1) settings.

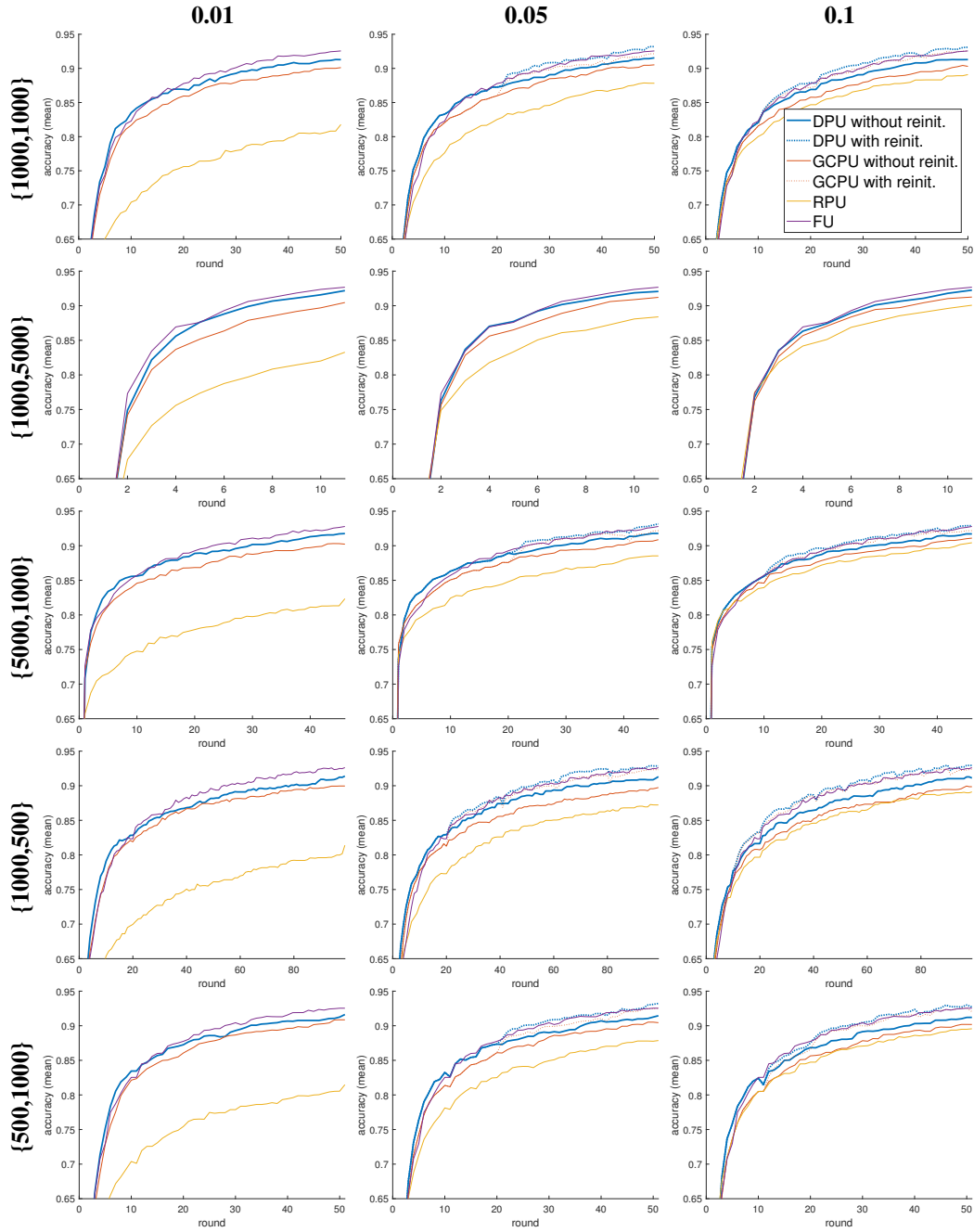


Figure 10: Comparison w.r.t. the mean accuracy under different $\{|\mathcal{D}^1|, |\delta\mathcal{D}^r|\}$ and updating ratio (0.01, 0.05 and 0.1) settings.

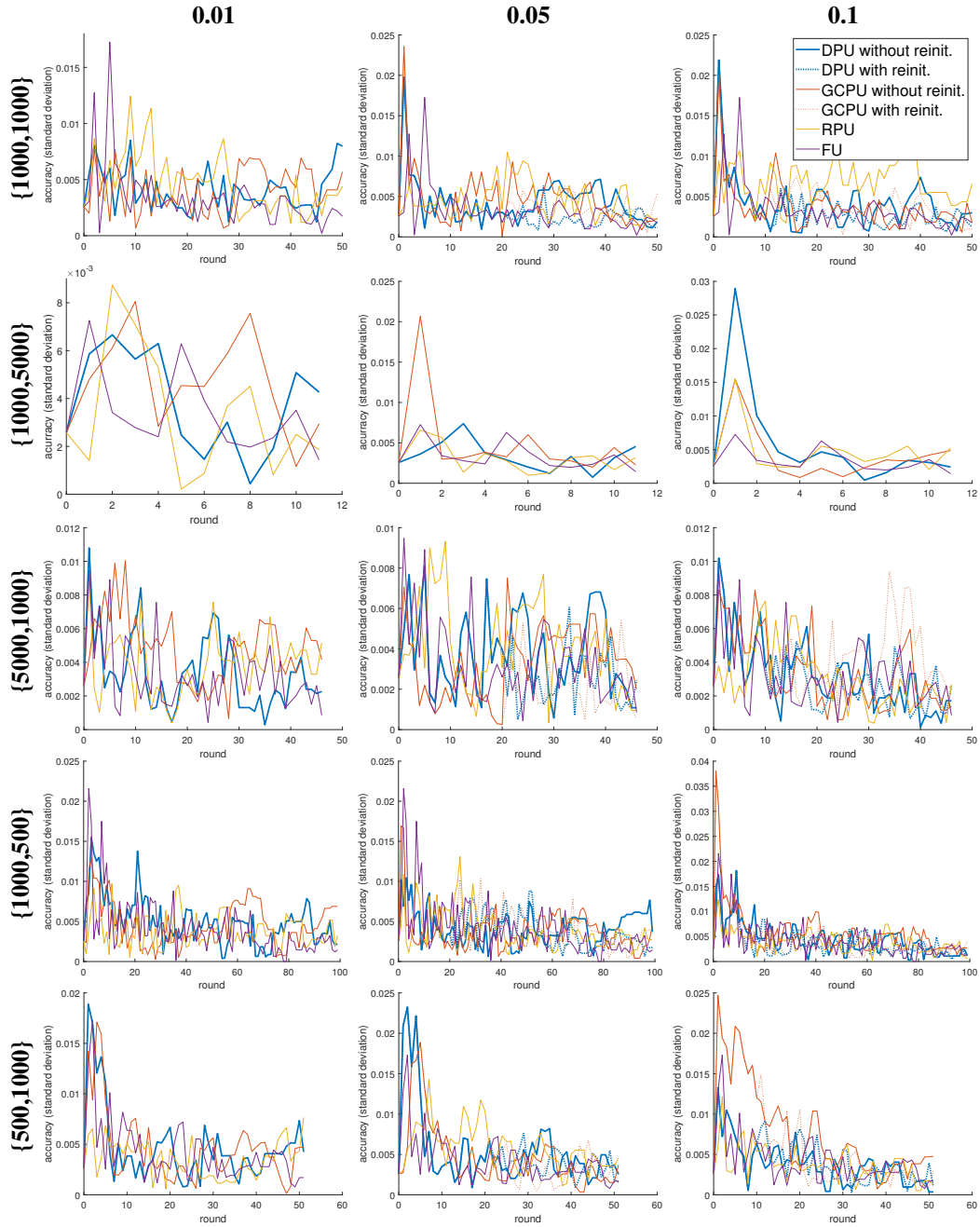


Figure 11: Comparison w.r.t. the standard deviation of accuracy under different $\{|\mathcal{D}^1|, |\delta\mathcal{D}^r|\}$ and updating ratio (0.01, 0.05 and 0.1) settings.